

# ReRoPE: Repurposing RoPE for Relative Camera Control

CHUNYANG LI\*, Zhejiang University, China  
 YUANBO YANG\*, Zhejiang University, China  
 JIAHAO SHAO\*, Zhejiang University, China  
 HONGYU ZHOU, Zhejiang University, China  
 KATJA SCHWARZ, Independent Researcher, Germany  
 YIYI LIAO†, Zhejiang University, China



Fig. 1. ReRoPE enables precise relative camera control for both image-to-video (Left) and video-to-video (Right) tasks by repurposing the redundant low-frequency bands of RoPE.

Video generation with controllable camera viewpoints is essential for applications such as interactive content creation, gaming, and simulation. Existing methods typically adapt pre-trained video models using camera poses relative to a fixed reference, e.g., the first frame. However, these encodings lack shift-invariance, often leading to poor generalization and accumulated drift. While relative camera pose embeddings defined between arbitrary view pairs offer a more robust alternative, integrating them into pre-trained video diffusion models without prohibitive training costs or architectural changes remains challenging. We introduce ReRoPE, a plug-and-play framework that incorporates relative camera information into pre-trained video diffusion models without compromising their generation capability. Our approach is based on the insight that Rotary Positional Embeddings (RoPE) in existing models underutilize their full spectral bandwidth, particularly in the low-frequency components. By seamlessly injecting relative camera pose information into these underutilized bands, ReRoPE achieves precise control while preserving strong pre-trained generative priors. We evaluate our method on both image-to-video (I2V) and video-to-video (V2V) tasks in terms of camera control accuracy and visual fidelity. Our results demonstrate that ReRoPE

\*Equal contribution

†Corresponding author

Authors' Contact Information: Chunyang Li, Zhejiang University, China; Yuanbo Yang, Zhejiang University, China; Jiahao Shao, Zhejiang University, China; Hongyu Zhou, Zhejiang University, China; Katja Schwarz, Independent Researcher, Germany; Yiyi Liao, Zhejiang University, China.

offers a training-efficient path toward controllable, high-fidelity video generation. See project page for more results: <https://sisyphe-lee.github.io/ReRoPE/>

CCS Concepts: • Computing methodologies → Computer vision.

Additional Key Words and Phrases: relative camera control, rotary position embeddings, diffusion models, pose estimation

## 1 Introduction

Camera control is a fundamental capability desired for video generation models, enabling explicit manipulation of viewpoint while preserving scene identity and temporal consistency. This functionality is essential for applications such as interactive content creation, gaming, and robotics simulation, which require the ability to direct complex cinematic sequences or synthesize diverse perspectives for virtual environments.

Most existing video generation models achieve camera control by injecting 6-DoF poses or ray features through a camera pose encoder [Bian et al. 2025; He et al. 2024; Ren et al. 2025; Yang et al. 2025]. These poses define the camera's rotation and translation of all cameras in the trajectory relative to a fixed reference frame, typically the first frame. While this provides explicit viewpoint conditioning, it ties video generation to a specific global reference, limiting generalization to unseen camera trajectories or shifted reference frames. A more robust approach should instead focus on

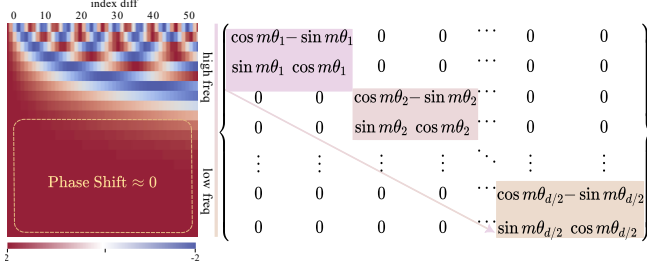


Fig. 2. Toy Case Analysis of RoPE. The heatmap shows attention scores of unit key and query vectors across different frequencies and index distances, revealing that low-frequency bands exhibit negligible phase shifts ( $\approx 0$ ) across the window.

the relative pose change between *any viewpoint pairs* along the trajectory, capturing how the scene appearance evolves based on local camera motion rather than a fixed global coordinate system. This principle aligns with the design of Rotary Positional Encoding (RoPE) [Barbero et al. 2025; Su et al. 2021], which has become the standard in large-scale transformers by shifting from absolute to relative positional representations. This is achieved by applying position-dependent rotations to hidden features, ensuring that the inner product between tokens depends only on their relative *temporal* or *spatial* distance. Since most state-of-the-art video models already employ RoPE, a natural question arises: can we reformulate camera control as a relative signal within this existing relative positional encoding framework?

Prior works have shown that camera parameters can be treated as a form of relative positional encoding similar to RoPE, where 3D transformations between views are injected into the attention mechanism [Li et al. 2025; Miyato et al. 2024]. However, these methods typically require training from scratch because they necessitate a fundamental re-partitioning of the RoPE structure. Specifically, RoPE-based video models divide feature vectors into blocks, where each block represents a 1D rotation corresponding to either the temporal, height, or width dimensions. To incorporate camera transformations, existing methods [Li et al. 2025] often re-allocate these blocks to represent 3D transformations (e.g.,  $SO(3)$  or  $SE(3)$ ), a configuration that is structurally incompatible with the 1D rotary priors of pre-trained models. Consequently, adopting these relative strategies has historically required re-learning the entire attention mechanism [Li et al. 2025; Miyato et al. 2024]. In contrast, training large-scale video diffusion models from scratch is prohibitively expensive, creating a clear demand for methods that can introduce robust camera control while preserving pre-trained architectural priors to ensure rapid convergence and minimal overhead.

We introduce ReRoPE, a plug-and-play framework that integrates relative camera information directly into the RoPE modules of a pre-trained video diffusion transformer. Our approach is based on the insight that the RoPE in pre-trained video diffusion models underutilizes its full spectral bandwidth. Specifically, we identify that the low-frequency components of both temporal and spatial RoPE are highly redundant for capturing relative positional differences. This redundancy is particularly prominent for the temporal

dimension, as the temporal sequence length in the latent space of modern video diffusion transformers is typically shorter than the spatial sequence length. Consequently, the temporal RoPE operates primarily in a regime where positional offsets are small, yielding more redundancy compared to the spatial dimensions. Leveraging this observation, ReRoPE is designed to be intentionally minimal. It requires no modifications to the transformer backbone, no auxiliary camera encoders, and no additional regression heads to interpret camera signals. Instead, relative camera geometry is encoded within a carefully selected subset of these low-frequency temporal channels, leaving the spatial RoPE and high-frequency temporal features untouched. This design ensures that ReRoPE remains fully compatible with existing architectures while strictly preserving pre-trained generative priors. Consequently, our method enables the adaptation of existing models into camera-controllable versions, supporting both image-to-video and video-to-video tasks within a short fine-tuning duration.

Our contributions are three-fold: (1) We identify a consistent low-frequency redundancy within the factorized spatio-temporal RoPE of video transformers, validated through a toy case study and experimental evaluation across three state-of-the-art backbones. (2) Based on this finding, we propose a simple yet effective mechanism to inject relative camera information into these redundant low-frequency bands, achieving high-precision camera control while preserving the pre-trained model’s generative priors. (3) Our approach is a plug-and-play module applicable to both video-to-video and image-to-video tasks, where it demonstrates superior camera controllability while maintaining high visual fidelity.

## 2 Related Work

*Video Generation Models.* Driven by recent progress in the formulation of generative models like diffusion [Ho et al. 2020] and flow matching [Lipman et al. 2022], video generation models [Ali et al. 2025; Blattmann et al. 2023a,b; HaCohen et al. 2024; Hong et al. 2022; Kong et al. 2024b; Wan et al. 2025] have achieved remarkable progress. While earlier methods [Blattmann et al. 2023a,b] adopt U-Net architecture, more recent models [Blattmann et al. 2023a; HaCohen et al. 2024; Hong et al. 2022; Kong et al. 2024b; Wan et al. 2025], such as Wan2.1 [Wan et al. 2025], switch to Diffusion Transformers (DiT) [Peebles and Xie 2022] with full attention mechanisms, achieving impressive performance. Despite these advances, controllability remains essential for downstream applications. While many recent works [Hu et al. 2025; Jiang et al. 2025] have achieved diverse control based on pretrained models like style and motion transfer, they still lack the capability for precise camera control.

*Camera Control Generation.* Precise camera motion control in generative models follows three primary strategies. Latent-based methods [Guo et al. 2023; Luo et al. 2025; Sun et al. 2025] utilize weight manipulation (e.g., LoRA) or pattern learning but often lack the explicit geometric constraints required for precise trajectory following. Geometry-guided methods enforce consistency via geometric priors, such as noise warping [Seo et al. 2024] or point cloud projection from depth estimations [Bai et al. 2025a; Cao et al. 2025; Duan et al. 2025; Huang et al. 2025b; Müller et al. 2024; Ren et al. 2025; Schneider et al. 2025; Wu et al. 2025; Yu et al. 2025a, 2024a,

2025b, 2024b]. However, these are strictly limited by depth estimation accuracy, which is non-trivial for dynamic scenes. The third line of methods bypasses structural estimation by directly injecting camera parameters. These include ray-based approaches [He et al. 2024; Van Hoorick et al. 2024], which convert 6DoF poses into Plücker ray maps for pixel-wise guidance via adapters, and parameter-based approaches [Bai et al. 2025b; Huang et al. 2025a; Wang et al. 2024], which fuse encoded extrinsics with visual features. Most such methods define poses relative to a fixed reference (usually the first frame), which is inherently restrictive. We instead propose that relative camera position encodings between *any* two views provide a more scalable and natural integration for controllable video generation.

*Relative Positional Encoding.* Rotary Positional Embedding (RoPE) [Su et al. 2021] establishes a standard for incorporating relative positional information in Transformers. By rotating query and key vectors based on their positions, RoPE enforces attention to depend strictly on relative distances. This property has driven its adoption across Large Language Models (LLMs) [Dubey et al. 2024; Liu et al. 2024; QwenTeam 2024; Touvron et al. 2023] and Vision Transformers (ViTs) [Heo et al. 2024; Labs 2024; Siméoni et al. 2025; Wang et al. 2025a]. For video generation, the RoPE mechanism also becomes the default choice for modeling the spatial and temporal positions of the visual tokens [Guo et al. 2025]. Inspired by RoPE, recent studies [Kong et al. 2024a; Li et al. 2025; Miyato et al. 2024] explore encoding camera relationships through relative embeddings. For instance, PRoPE [Li et al. 2025] injects camera intrinsics and extrinsics into the self-attention, modeling camera pose as a relative transformation between views. While most of these methods focus on training from scratch to learn the attention with relative camera embedding, concurrent works like BulletTime [Wang et al. 2025b] and UCPE [Zhang et al. 2025b] pursue similar directions to ours by injecting relative camera information into the existing RoPE of pre-trained video models. However, these approaches typically rely on additional learnable weights or auxiliary modules to accommodate the new pose encodings, whereas our method requires no architectural changes based on our findings in the low-frequency redundancy.

### 3 Preliminary

*Rotary Position Encoding (RoPE).* Originally developed for Large Language Models (LLMs) to capture long-range dependencies [Su et al. 2021], RoPE encodes position via feature rotation, ensuring attention depends only on relative token distance. Let  $q_i, k_j \in \mathbb{R}^d$  be query and key vectors at positions  $i$  and  $j$  with head dimension  $d$ . RoPE treats the vector as  $d/2$  independent 2D planes, rotating each with a frequency  $\omega_f = \theta^{-2f/d}$  where  $\theta = 10^4$  and  $f = \{0, \dots, d/2-1\}$ .

Let  $\Phi_2(\phi) = \begin{bmatrix} \cos \phi & -\sin \phi \\ \sin \phi & \cos \phi \end{bmatrix}$  denote the  $2 \times 2$  rotation, the full rotation matrix for position  $m$  is defined as:

$$\Phi(m) = \text{blkdiag}(\Phi_2(m\omega_0), \dots, \Phi_2(m\omega_{d/2-1})), \quad (1)$$

where  $\text{blkdiag}(\mathbf{A}, \mathbf{B}) = \begin{bmatrix} \mathbf{A} & \mathbf{0} \\ \mathbf{0} & \mathbf{B} \end{bmatrix}$  denotes a block-diagonal matrix with  $\mathbf{A}$  and  $\mathbf{B}$  on its main diagonal, see Fig. 2. The encoded vectors

$\tilde{q}_i = \Phi(i) q_i$  and  $\tilde{k}_j = \Phi(j) k_j$  satisfy  $\langle \tilde{q}_i, \tilde{k}_j \rangle = \langle q_i, \Phi(i-j) k_j \rangle$ . Thus, attention logits depend on the relative offset  $i - j$  rather than absolute indices, providing translation invariance and better length extrapolation.

*RoPE for Videos.* Video diffusion transformers, e.g., Wan [Wan et al. 2025] and CogVideoX [Hong et al. 2022], extend RoPE to the 3D token grid of temporal ( $\tau$ ), height ( $h$ ), and width ( $w$ ) coordinates using a factorized approach. The head dimension  $d$  is partitioned into three disjoint channel bands  $d = d_\tau + d_h + d_w$ , with each band independently encoding a single axis in  $(\tau, h, w)$ . Let  $\Phi_\tau(\cdot)$ ,  $\Phi_h(\cdot)$ , and  $\Phi_w(\cdot)$  be the rotation operators defined as in Eq. (8) for each band. The 3D rotation operator is the block-diagonal concatenation of these per-axis rotations:

$$\Phi^{\text{ViT}}(\tau, h, w) = \text{blkdiag}(\underbrace{\Phi_\tau(\tau)}_{d_\tau}, \underbrace{\Phi_h(h)}_{d_h}, \underbrace{\Phi_w(w)}_{d_w}), \quad (2)$$

where  $d_\tau = d_h = d_w = d/3$  is a common choice for popular video diffusion models [Hong et al. 2022; Wan et al. 2025]. By the orthogonality of the block-diagonal structure, the inner product between two tokens at coordinates  $(\tau, h, w)$  and  $(\tau', h', w')$  depends solely on their relative spatio-temporal offsets  $(\Delta\tau, \Delta h, \Delta w)$ .

*Cameras as Relative Positional Encoding.* Similar to RoPE for videos, GTA [Miyato et al. 2024] and PRoPE [Li et al. 2025] adopt a factorized construction of the rotation matrix  $\Phi$  for viewpoint interpolation between posed input frames. Specifically, they allocate a disjoint band of the head dimension to represent relative camera transformations. The remaining channels encode the relative spatial location  $(h, w)$ . Let  $\mathbf{P}_c = \mathbf{K}_c[\mathbf{R}_c \mid \mathbf{t}_c]$  denote the  $3 \times 4$  projection matrix of a camera  $c$ , which is lifted to a  $4 \times 4$  homogeneous matrix:

$$\tilde{\mathbf{P}}_c = \begin{bmatrix} \mathbf{K}_c \mathbf{R}_c & \mathbf{K}_c \mathbf{t}_c \\ \mathbf{0}^\top & 1 \end{bmatrix}. \quad (3)$$

For a token at camera position  $\tilde{\mathbf{P}}_c$ , the camera information is injected via a block-diagonal transformation  $\Phi^{\text{PRoPE}}(c, h, w) \in \mathbb{R}^{d \times d}$ :

$$\Phi^{\text{PRoPE}}(c, h, w) = \text{blkdiag}(\underbrace{\Phi_{\text{proj}}(c)}_{d_c}, \underbrace{\Phi_h(h)}_{d_h}, \underbrace{\Phi_w(w)}_{d_w}) \quad (4)$$

where  $d_c = d/2$  and  $d_h = d_w = d/4$  in PRoPE [Li et al. 2025]. Here,  $\Phi_{\text{proj}}(c)$  is constructed by repeating the lifted camera matrix  $\tilde{\mathbf{P}}_c$  along the diagonal:

$$\Phi_{\text{proj}}(c) = \text{blkdiag}(\tilde{\mathbf{P}}_c, \dots, \tilde{\mathbf{P}}_c) \in \mathbb{R}^{d_c \times d_c}. \quad (5)$$

and  $\tilde{\mathbf{P}}_c$  is the lifted matrix for the camera at index  $c$ . By partitioning the head dimension this way, the attention mechanism computes the relative transformation between any two tokens at positions  $c$  and  $t$ :

$$\mathcal{P}_{c \leftarrow t} = \tilde{\mathbf{P}}_c \tilde{\mathbf{P}}_t^{-1}. \quad (6)$$

Since  $\mathcal{P}_{c \leftarrow t}$  depends only on the camera pair, it encodes a signal suitable for relative positional modeling. However, as can be observed, the spatial-temporal RoPE design in Eq. (9) and the camera-projection design in Eq. (4) utilize different channel-wise structures. This architectural discrepancy makes it difficult to directly merge relative camera pose embeddings into pre-trained video models without disrupting their generative priors.

## 4 ReRoPE

### 4.1 Overview and setting.

Our goal is to enable precise camera control within a pre-trained video diffusion transformer. We consider two distinct generative settings: 1) Video-to-Video (V2V): Given an input video sequence and its corresponding source camera trajectory, the task is to re-render or adapt the video content to follow a new, user-defined target camera trajectory. 2) Image-to-Video (I2V): Given a single reference frame, the model synthesizes a video sequence that adheres to a specified target camera trajectory.

We build upon a pre-trained video diffusion transformer operating on a 3D latent grid of  $T \times H \times W$  tokens. The model employs a multi-head attention mechanism with head dimension  $d = d_\tau + d_h + d_w$ , split into factorized temporal, vertical, and horizontal RoPE bands. We denote the temporal index by  $\tau \in \{0, \dots, T-1\}$  and the spatial indices by  $(h, w)$ .

### 4.2 Low-Frequency Redundancy of RoPE

As discussed in Sec. 3, it is non-trivial to inject the relative camera pose into the existing RoPE matrix without disrupting the original generative video prior. Therefore, we first look into the original RoPE and analyze its behavior.

*Toy Case of Frequency Bands.* Inspired by [Barbero et al. 2025], which demonstrates that attention mechanisms of LLMs often use only a subset of RoPE frequency bands, we investigate the specific impact of different bands on video generation.

We design a toy experiment. Consider two-dimensional query and key tokens at temporal positions  $i$  and  $j$ . To isolate the effect of the rotation, we set all features to a constant unit vector  $q_i = k_j = [1, 1]^\top$ . The resulting attention score  $A$  after the RoPE operation  $\Phi_2$  is defined by the inner product:

$$\begin{aligned} A(i, j, \omega_k) &= \langle \Phi_2(i\omega_k)q_i, \Phi_2(j\omega_k)k_j \rangle \\ &= \langle q_i, \Phi_2((i-j)\omega_k)k_j \rangle = 2 \cos((i-j)\omega_k), \end{aligned} \quad (7)$$

where  $\omega_k = \theta^{-2f/d}$  with  $\theta = 10^4$  and  $f = \{0, \dots, d/2-1\}$ . For our experiment, we use common values in video transformers, considering 50 frames, i.e.,  $i, j \in \{0, \dots, 49\}$ , and a base frequency of  $\theta = 10^4$ . We visualize frequency bands indexed from high to low frequency on the x-axis and the relative distance between temporal positions  $\Delta\tau = i - j$  on the y-axis in Fig. 2 (left).

The resulting heatmap reveals an oscillatory attention signal where high-frequency bands (small  $f$ ) shift phase rapidly, providing fine-grained positional discrimination. Conversely, low-frequency bands (large  $f$ ) remain nearly constant across standard video lengths, with values approaching the dot product  $\langle [1, 1]^\top, [1, 1]^\top \rangle = 2$ . This indicates that these low-frequency components are underutilized for positional encoding in pre-trained models. This redundancy suggests that the low-frequency subspace of  $\Phi_\tau$  can be repurposed for camera geometry without disrupting the temporal ordering captured by higher frequencies.

*Disabling Frequency Bands in Video DiTs.* To further examine the effect of different frequency bands in trained video diffusion models, we investigate the behavior of “masking out” low-frequency bands



Fig. 3. Frequency analysis across three video diffusion models [Hong et al. 2022; Kong et al. 2024b; Wan et al. 2025]. We observe that masking high-frequency bands (Left) leads to model collapse, whereas masking low-frequency bands (Middle) maintains generation quality comparable to the baseline (Right), confirming the functional redundancy of low-frequency components.

on three well-known models: Wan 2.1 [Wan et al. 2025], Wan 2.1-I2V, and CogVideoX [Hong et al. 2022]. We set the rotary matrix to the identity for the low-frequency subspace corresponding to  $f \in \{d_\tau/4, \dots, d_\tau/2-1\}$ :

$$\Phi(m) = \text{blkdiag}(\underbrace{\Phi_2(m\omega_0), \dots, \Phi_2(m\omega_{d_\tau/4-1})}_{d_\tau/2}, \underbrace{\mathbf{I}}_{d_\tau/2}), \quad (8)$$

This masking is applied to all spatial and temporal RoPE components, i.e., to  $\Phi_\tau(\tau)$ ,  $\Phi_h(h)$ , and  $\Phi_w(w)$ . As shown in Fig. 3, the videos generated with this “masking” remain nearly identical to their original counterparts, indicating that the models do not rely on these bands for discriminating relative positions. In contrast, masking out the high-frequency bands ( $f \in \{0, \dots, d/4-1\}$ ) significantly degrades the model’s performance. This empirical result further corroborates our key insight that a substantial portion of the RoPE head dimension is functionally redundant and can be repurposed for external control signals like camera geometry.

### 4.3 ReRoPE: Repurposing RoPE for Camera Control

We now repurpose the temporal low-frequency subspace to carry camera information, while preserving the original RoPE behavior on all remaining channels, as shown in Fig. 4. While our analysis also identifies redundancy in the spatial embeddings, we focus on applying ReRoPE to the temporal dimension, because the (latent) number of frames is typically smaller than the (latent) spatial resolution. E.g.,  $T = 21, H = 30, W = 52$  for Wan2.1 [Wan et al. 2025], meaning that the temporal embeddings contain the highest redundancy.

*ReRoPE at Temporal RoPE.* Our proposed solution is simple: we keep the standard temporal RoPE on the high-frequency bands, and replace the low-frequency band with relative camera information. For the relative camera, we follow PRoPE to construct the projection block as shown in Eq. 4). Let  $d_L$  denote the dimensionality of the temporal low-frequency subspace we choose to repurpose, which is a value that is divisible by 4. The repurposed temporal operator is

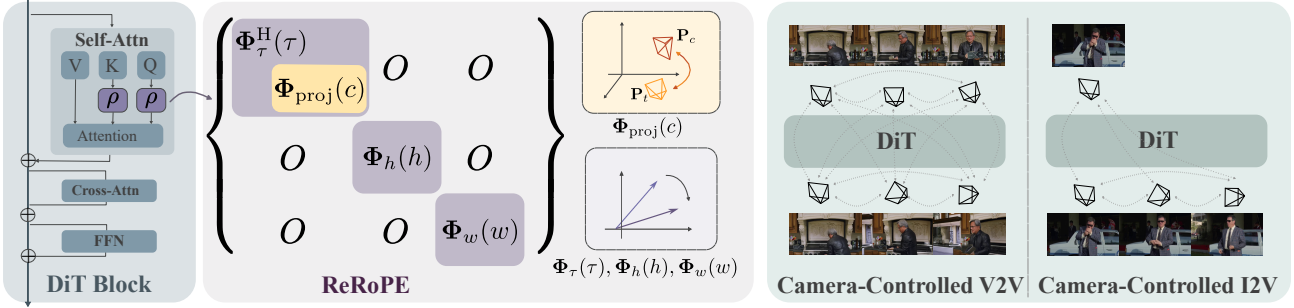


Fig. 4. Overview of ReRoPE framework. We enable relative camera control by repurposing the redundant low-frequency temporal bands of a pre-trained Video DiT. (Left and Middle) As shown in the matrix decomposition, we retain spatial and high-frequency temporal bands to preserve generative priors, replacing only the underutilized low-frequency temporal bands with our camera projection block. (Right) This plug-and-play mechanism supports both Video-to-Video and Image-to-Video tasks.

$$\Phi^{\text{ReRoPE}}(\tau, c, h, w) = \text{blkdiag}\left(\underbrace{\Phi_{\tau}^H(\tau)}_{d_{\tau}^H}, \underbrace{\Phi_{\text{proj}}(c)}_{d_{\tau}^L}, \underbrace{\Phi_h(h)}_{d_h}, \underbrace{\Phi_w(w)}_{d_w}\right), \quad (9)$$

i.e., we only modify the temporal low-frequency bands and keep all spatial RoPE bands intact. Here,  $d_{\tau}^H = d_{\tau}^L = d/6$  in our experiments. Note that in contrast to the original RoPE operations, the relative camera encoding operation achieved via  $\Phi_{\text{proj}}(c)$  encodes the relative camera transformation  $P_{c \leftarrow t} = \tilde{P}_c \tilde{P}_t^{-1}$  between any pair of cameras  $c$  and  $t$ , which is non-norm-preserving. Therefore, we stabilize training by normalizing the translation component when constructing  $\tilde{P}_c$  and  $\tilde{P}_t$ , as detailed in Sec. 4.4.

#### 4.4 Training

We fine-tune the pre-trained video diffusion transformer to incorporate explicit camera control. We train our models for Video-to-Video (V2V) and Image-to-Video (I2V) settings, respectively.

*Conditioning Strategy.* In the V2V setting, we treat generation as conditional video inpainting. We concatenate the latent representations of the source and target videos along the temporal dimension, applying the diffusion process exclusively to target frames. This setup forces the model to learn geometric correlations across all source-source, source-target, and target-target view pairs based on their relative camera trajectories. For I2V, the first frame serves as a noise-free visual anchor, and the model predicts the noise for the subsequent sequence. To support Classifier-Free Guidance (CFG) [Ho and Salimans 2022] during inference, we apply a 10% dropout rate to text prompts during training.

*Relative Pose Normalization.* To ensure relative camera transformations are meaningful across all view pairs, we define source and target poses within a unified coordinate system. Specifically, in V2V, the first frame of the condition sequence serves as the origin for both trajectories, while in I2V, poses are relative to the input image frame. To resolve scale ambiguity across diverse scenes, we normalize all translation vectors by the maximum  $L_2$  norm of translations within the training sequence. This yields a scale-invariant pose representation compatible with our ReRoPE injection.

*Objective and Optimization.* We freeze all parameters of the pre-trained backbone except for the self-attention layers, allowing the model to adapt to the new positional embedding mechanism without forgetting its generative prior. The model is optimized using the flow matching objective [Lipman et al. 2022], computed as the Mean Squared Error (MSE) loss between the predicted and ground-truth flow velocity. We use the AdamW optimizer with a learning rate of 1e-5 and gradient clipping of 0.05.

## 5 Experiments

We evaluate ReRoPE on camera-controlled video generation. We first describe the experimental setup in §5.1, then compare against state-of-the-art baselines on camera controllable video-to-video (V2V) and image-to-video (I2V) settings (§5.2–§5.3). Finally, we present ablations on key design choices in §5.4.

### 5.1 Experimental Setup

We employ Wan2.1 and Wan2.2 as our base video diffusion transformers for the V2V and I2V tasks, respectively, modifying only the temporal low-frequency RoPE bands while keeping the denoising architecture intact. For V2V, we train on the calibrated MultiCamVideo [Bai et al. 2025b] dataset; for I2V, we jointly train on MultiCamVideo, SDG-1.5M [Huang et al. 2025c] (annotated via VIPE [Huang et al. 2025c]), and DL3DV [Ling et al. 2024]. The models are trained for 10,000 iterations on 8 NVIDIA RTX 5880 GPUs, requiring approximately one day for V2V and 2~3 days for I2V. Performance is evaluated using: (i) camera accuracy via pose errors (RRE/RTE/ATE) estimated by VIPE, (ii) video quality and consistency through VBench [Huang et al. 2024] sub-metrics, and (iii) geometric fidelity via View Synchronization (View Syn). View Syn uses GIM [Shen et al. 2024] to calculate the average number of matched pixel pairs per frame with high confidence between generated and ground truth frames. For our ablation studies, we additionally report FID [Heusel et al. 2017] and FVD [Unterthiner et al. 2018].

### 5.2 V2V: Comparison to Baselines

We evaluate video-to-video (V2V) camera control on 200 videos sampled from SDG-1.5M. All methods use identical conditioning



Fig. 5. Qualitative comparison of V2V generation. Trajectory visualization shows that baselines (red) deviate from the ground truth (green). In contrast, ReRoPE (blue) maintains tight alignment, demonstrating the precise geometric control required for superior visual fidelity and consistency.

Method	Camera Accuracy			VBench					View Syn↑
	RRE↓	RTE↓	ATE↓	subject consistency↑	background consistency↑	motion smoothness↑	dynamic degree↑	aesthetic quality↑	
TrajectoryCrafter [Yu et al. 2025b]	1.1693	0.0741	0.3824	<b>0.9406</b>	<b>0.9549</b>	0.9842	0.4426	<b>0.6176</b>	0.6174
ReCamMaster [Bai et al. 2025b]	0.7758	0.2434	0.4814	0.9270	0.9333	<b>0.9904</b>	0.8985	0.5831	0.6497
ReRoPE (Ours)	<b>0.7416</b>	<b>0.0629</b>	<b>0.1853</b>	0.9258	0.9319	<b>0.9904</b>	<b>0.9045</b>	0.5824	<b>0.6583</b>

Table 1. V2V camera control on SDG-1.5M [Huang et al. 2025c] (200 sampled videos). We report camera pose errors (RRE/RTE/ATE), VBench sub-metrics, and View Syn. ↑ higher is better, ↓ lower is better.

videos, target trajectories, prompts, and seeds to ensure a fair comparison, and none of them has been trained on SDG-1.5M for the V2V setting. We compare ReRoPE against two state-of-the-art baselines, TrajectoryCrafter [Yu et al. 2025b] and ReCamMaster [Bai et al. 2025b], as shown in Table 1 and Fig. 5. TrajectoryCrafter relies on estimating the depth of the input to construct a dynamic point cloud, followed by explicit reprojection to achieve camera control. While this approach achieves superior aesthetic quality, it is highly sensitive to depth estimation errors, and inaccuracies in the global point cloud lead to lower camera accuracy. In contrast, ReRoPE avoids explicit geometric conditioning, reflecting in higher camera accuracy. ReCamMaster is more closely related to our framework, as it also avoids explicit geometry conditioning by projecting camera parameters through an encoder and adding them directly to the transformer’s intermediate features. However, our results show that ReRoPE achieves superior camera controllability by encoding the relative relationship between any pair of cameras within the RoPE subspace while maintaining competitive perceptual quality. Fig. 9 further illustrates our V2V results under various camera trajectories.

### 5.3 I2V: Comparison to Baselines

We evaluate ReRoPE for I2V camera control on DL3DV [Ling et al. 2024] (static scenes) and SDG-1.5M [Huang et al. 2025c] (featuring dynamic subjects). A key advantage of our approach is the ability to simultaneously model camera motion and object dynamics. In contrast, existing baselines are largely limited to static viewpoint transfer, where dynamic subjects appear as rigid “frozen” scans. Because pose estimation algorithms struggle to decouple camera

movement from scene motion in dynamic videos, quantitative metrics become unreliable for comparing rigid vs. non-rigid outputs. Therefore, we restrict our quantitative comparison to the static scenes of DL3DV to ensure a fair evaluation of camera accuracy. Specifically, we compare our model with two state-of-the-art baselines: SEVA [Zhou et al. 2025] and DualCamCtrl [Zhang et al. 2025a]. Both inject camera information using Plücker ray parameterization, where DualCamCtrl further incorporates monocular depth cues. As shown in Table 2, our method achieves the highest camera accuracy while maintaining comparable video fidelity. Beyond quantitative metrics, we provide qualitative comparisons on SDG-1.5M in Fig. 6, as well as more results in Fig. 10 and Fig. 11. While baseline methods are restricted to changing the viewpoint of a frozen scene, ReRoPE successfully generates dynamic subjects that adhere to the text prompt while following the specified camera trajectory.

### 5.4 Ablation

We ablate key design choices of ReRoPE under the same I2V evaluation protocol as in §5.3.

Beyond our proposed low-frequency injection, we consider two alternatives for integrating relative camera information into the pre-trained backbone: 1) Full-Temporal Replacement, which entirely replaces the temporal RoPE with the camera projection term, discarding original temporal frequencies; and 2) Double RoPE, which first applies the standard spatio-temporal RoPE from Eq. (9), followed by an additional operation that replaces only the temporal component with the camera projection. This effectively rotates temporal features twice, first for positional encoding and then for camera



Fig. 6. Qualitative comparison on dynamic I2V scenes showing that ReRoPE synthesizes natural object motion, whereas baselines incorrectly render the subject as a static rigid body.

Method	Camera Accuracy			VBench					
	RRE↓	RTE↓	ATE↓	subject consistency↑	background consistency↑	motion smoothness↑	dynamic degree↑	aesthetic quality↑	imaging quality↑
SEVA [Zhou et al. 2025]	0.2767	0.0642	0.3183	0.9334	0.9445	0.9766	0.2980	<b>0.5431</b>	0.6384
DualCamCtrl [Zhang et al. 2025a]	0.1080	0.0103	0.0909	0.9543	<b>0.9462</b>	0.9846	-	0.5163	<b>0.7084</b>
ReRoPE (Ours)	<b>0.0886</b>	<b>0.0078</b>	<b>0.0703</b>	<b>0.9638</b>	0.9403	<b>0.9896</b>	<b>0.5587</b>	0.5382	0.7020

Table 2. I2V camera control evaluated on a test set composed of **DL3DV**. We report camera pose errors (RRE/RTE/ATE) and VBench sub-metrics. ↑ higher is better, ↓ lower is better.

Setting	FID↓	FVD↓	Aesthetic Quality↑	Imaging Quality↑
w/o normalization	185.6123	110.8156	0.3495	0.4698
w/ normalization (Ours)	85.8568	59.4710	0.5671	0.6357

Table 3. Ablation on translation normalization.

transformation, while maintaining standard RoPE for spatial dimensions. As shown in Fig. 7, our method achieves the best FID with the fastest convergence, demonstrating that it effectively preserves the pre-trained video generation prior. In contrast, Full-Temporal Replacement disrupts the backbone’s learned temporal prior, while Double RoPE forces the same channels to encode both temporal position and camera geometry. This creates signal interference that compromises both camera accuracy and perceptual quality. We provide a qualitative comparison in Fig. 8 and additional comparisons on more metrics in the supplementary material.

Second, we ablate translation normalization of the camera matrices. In this study, we compare ReRoPE with and without translation normalization, while keeping the same PROPE injection strategy. Without normalization, large translation magnitudes in the projective block can inflate attention logits and destabilize conditioning, especially under larger baselines. Table 3 confirms this effect: enabling translation normalization consistently improves camera fidelity (lower RRE/RTE/ATE) and yields better FVD, indicating more stable and higher-quality generation under projective conditioning.

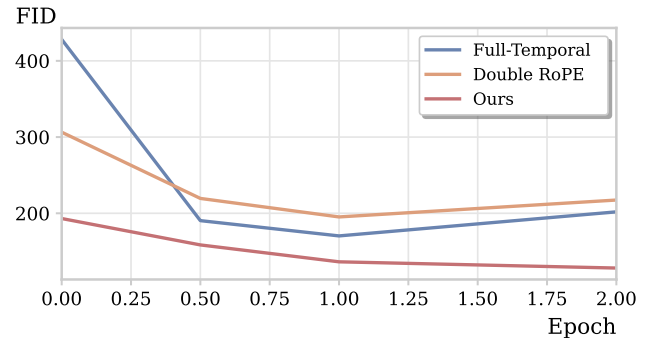


Fig. 7. Training convergence comparison. FID scores over training epochs show that ReRoPE converges faster and reaches a significantly lower final FID than the Full-Temporal Replacement and Double RoPE baselines.

## 6 Conclusion

We recast camera control as a relative positional-encoding problem, leveraging the spectral redundancy inherent in pre-trained video transformers. By injecting camera geometry into the underutilized low-frequency temporal subspace of RoPE, ReRoPE provides a unified, plug-and-play framework applicable to both V2V and I2V tasks. This approach preserves pre-trained generative priors, enabling precise control over complex trajectories without necessitating architectural changes. Our evaluations across diverse datasets demonstrate that ReRoPE achieves superior camera accuracy and 3D consistency while maintaining high visual fidelity.

## References

Arslan Ali, Junjie Bai, Maciej Bala, Yogesh Balaji, Aaron Blakeman, Tiffany Cai, Jiaxin Cao, Tianshi Cao, Elizabeth Cha, Yu-Wei Chao, et al. 2025. World simulation with video foundation models for physical ai. *arXiv preprint arXiv:2511.00062* (2025).

Jianhong Bai, Menghan Xia, Xiao Fu, Xintao Wang, Lianrui Mu, Jinwen Cao, Zuozhu Liu, Haoji Hu, Xiang Bai, Pengfei Wan, et al. 2025b. ReCamMaster: Camera-Controlled Generative Rendering from A Single Video. *arXiv preprint arXiv:2503.11647* (2025).

Yunpeng Bai, Haoxiang Li, and Qixing Huang. 2025a. Positional Encoding Field. *arXiv preprint arXiv:2510.20385* (2025).

Federico Barbero, Alex Vitvitsky, Christos Perivolaropoulos, Razvan Pascanu, and Petar Veličković. 2025. Round and Round We Go! What makes Rotary Positional Encodings useful? *arXiv:2410.06205* [cs.LG]

Weikang Bian, Yijin Li, Zhaoyang Huang, Fu-Yun Wang, Xiaoyu Shi, and Hongsheng Li. 2025. GS-DiT: Advancing Video Generation with Dynamic 3D Gaussian Fields through Efficient Dense 3D Point Tracking. In *Proceedings of the IEEE/CVF Conference on Computer Vision and Pattern Recognition (CVPR)*. IEEE, Nashville, TN, USA, 1–10.

Andreas Blattmann, Tim Dockhorn, Sumith Kulal, Daniel Mendelevitch, Maciej Kilian, Dominik Lorenz, Yam Levi, Zion English, Vikram Voleti, Adam Letts, et al. 2023a. Stable video diffusion: Scaling latent video diffusion models to large datasets. *arXiv preprint arXiv:2311.15127* (2023).

Andreas Blattmann, Robin Rombach, Huan Ling, Tim Dockhorn, Seung Wook Kim, Sanja Fidler, and Karsten Kreis. 2023b. Align your Latents: High-Resolution Video Synthesis with Latent Diffusion Models. In *IEEE Conference on Computer Vision and Pattern Recognition (CVPR)*.

Chenjie Cao, Jingkai Zhou, shikai Li, Jingyun Liang, Chaohui Yu, Fan Wang, Xiangyang Xue, and Yanwei Fu. 2025. Uni3C: Unifying Precisely 3D-Enhanced Camera and Human Motion Controls for Video Generation. *arXiv preprint arXiv:2504.14899* (2025).

Haoyi Duan, Yunzhi Zhang, Yilun Du, and Jiajun Wu. 2025. Ctrl-VI: Controllable Video Synthesis via Variational Inference. *arXiv preprint arXiv:2510.07670* (2025).

Abhimanyu Dubey, Abhinav Jauhri, Abhinav Pandey, Abhishek Kadian, Ahmad Al-Dahle, Aiesha Letman, Akhil Mathur, Alan Schelten, Amy Yang, Angela Fan, et al. 2024. The llama 3 herd of models. *arXiv preprint arXiv:2407.21783* (*Meta AI Technical Report*) (2024).

Yuwei Guo, Ceyuan Yang, Anyi Rao, Zhengyang Liang, Yaohui Wang, Yu Qiao, Maneesh Agrawala, Dahu Lin, and Bo Dai. 2023. AnimateDiff: Animate Your Personalized Text-to-Image Diffusion Models without Specific Tuning.

Yuwei Guo, Ceyuan Yang, Ziyan Yang, Zhibei Ma, Zhijie Lin, Zhenheng Yang, Dahu Lin, and Lu Jiang. 2025. Long Context Tuning for Video Generation. *arXiv:2503.10589* [cs.CV]

Yoav HaCohen, Nisan Chirrut, Benny Brazowski, Daniel Shalem, Dudu Moshe, Eitan Richardson, Eran Levin, Guy Shiran, Nir Zabari, Ori Gordon, Poriya Panet, Sapir Weissbuch, Victor Kulikov, Yaki Bitterman, Zevi Melumian, and Ofir Bibi. 2024. LTX-Video: Realtime Video Latent Diffusion. *arXiv preprint arXiv:2501.00103* (2024).

Hao He, Hao Zheng, Yinghao Xu, Tong Wang, Jun Wang, Hongsheng Li, and Ceyuan Yang. 2024. CameraCtrl: Enabling Camera Control for Text-to-Video Generation. *arXiv:2404.02101* [cs.CV]

Byeongho Heo, Song Park, Dongyoon Han, and Sangdoo Yun. 2024. Rotary Position Embedding for Vision Transformer. In *European Conference on Computer Vision (ECCV)*.

Martin Heusel, Hubert Ramsauer, Thomas Unterthiner, Bernhard Nessler, and Sepp Hochreiter. 2017. Gans trained by a two time-scale update rule converge to a local nash equilibrium. *Advances in neural information processing systems* 30 (2017).

Jonathan Ho, Ajay Jain, and Pieter Abbeel. 2020. Denoising Diffusion Probabilistic Models. In *Advances in Neural Information Processing Systems (NeurIPS)*, Vol. 33. Curran Associates, Inc., Virtual, 6840–6851.

Jonathan Ho and Tim Salimans. 2022. Classifier-free diffusion guidance. *arXiv preprint arXiv:2207.12598* (2022).

Wenyi Hong, Ming Ding, Wendi Zheng, Xinghan Liu, and Jie Tang. 2022. CogVideo: Large-scale Pretraining for Text-to-Video Generation via Transformers. *arXiv:2205.15868* [cs.CV]

Teng Hu, Zhentao Yu, Zhengguang Zhou, Sen Liang, Yuan Zhou, Qin Lin, and Qinglin Lu. 2025. HunyuanCustom: A Multimodal-Driven Architecture for Customized Video Generation. *arXiv:2505.04512* [cs.CV] <https://arxiv.org/abs/2505.04512>

Jiahui Huang, Qunjie Zhou, Hesam Rabeti, Aleksandr Korovkin, Huan Ling, Xuanchi Ren, Tianchang Shen, Jun Gao, Dmitry Slepichev, Chen-Hsuan Lin, Jiawei Ren, Kevin Xie, Joydeep Biswas, Laura Leal-Taixe, and Sanja Fidler. 2025c. ViPE: Video Pose Engine for 3D Geometric Perception. In *NVIDIA Research Whitepapers*.

Tianyu Huang, Wangguandong Zheng, Tengfei Wang, Yuhao Liu, Zhenwei Wang, Junta Wu, Jie Jiang, Hui Li, Rynson WH Lau, Wangmeng Zuo, and Chuncho Guo. 2025b. Voyager: Long-Range and World-Consistent Video Diffusion for Explorable 3D Scene Generation. *arXiv preprint arXiv:2506.04225* (2025).

Ziqi Huang, Yinan He, Jiaoshuo Yu, Fan Zhang, Chenyang Si, Yuming Jiang, Yuanhan Zhang, Tianxing Wu, Qingyang Jin, Nattapol Chanpaisit, Yaohui Wang, Xinyuan Chen, Limin Wang, Dahua Lin, Yu Qiao, and Ziwei Liu. 2024. VBench: Comprehensive Benchmark Suite for Video Generative Models. In *Proceedings of the IEEE/CVF Conference on Computer Vision and Pattern Recognition*.

Zhenning Huang, Hyeonho Jeong, Xuelin Chen, Yulia Gryaditskaya, Tuanfeng Y. Wang, Joan Lasenby, and Chun-Hao Huang. 2025a. SpaceTimePilot: Generative Rendering of Dynamic Scenes Across Space and Time. *arXiv preprint arXiv:2512.25075* (2025). <https://arxiv.org/abs/2512.25075>

Zeyinzi Jiang, Zhen Han, Chaojie Mao, Jingfeng Zhang, Yulin Pan, and Yu Liu. 2025. VACE: All-in-One Video Creation and Editing. In *Proceedings of the IEEE/CVF International Conference on Computer Vision*. 17191–17202.

Weijie Kong, Qi Tian, Zijian Zhang, Rov Min, Zuozhuo Dai, Jia Zhou, Jiangfeng Xiong, Xin Li, Bo Wu, Jianwei Zhang, et al. 2024b. Hunyuanvideo: A systematic framework for large video generative models. *arXiv preprint arXiv:2412.03603* (2024).

Xin Kong, Shikun Liu, Xiaoyang Lyu, Marwan Taher, Xiaojuan Qi, and Andrew J Davison. 2024a. Eschneret: A generative model for scalable view synthesis. In *Proceedings of the IEEE/CVF Conference on Computer Vision and Pattern Recognition*. 9503–9513.

Black Forest Labs. 2024. FLUX. <https://github.com/black-forest-labs/flux>.

Ruiling Li, Brent Yi, Junchen Liu, Hang Gao, Yi Ma, and Angjoo Kanazawa. 2025. Cameras as Relative Positional Encoding. *arXiv:2507.10496* [cs.CV]

Lu Ling, Yichen Sheng, Zhi Tu, Wentian Zhao, Cheng Xin, Kun Wan, Lantao Yu, Qianyu Guo, Zixun Yu, Yawen Lu, et al. 2024. DL3dv-10k: A large-scale scene dataset for deep learning-based 3d vision. In *Proceedings of the IEEE/CVF Conference on Computer Vision and Pattern Recognition*. 22160–22169.

Yaron Lipman, Ricky TQ Chen, Heli Ben-Hamu, Maximilian Nickel, and Matt Le. 2022. Flow matching for generative modeling. *arXiv preprint arXiv:2210.02747* (2022).

Aixin Liu, Bei Feng, Bing Xue, Bingxuan Wang, Bochao Wu, Chengda Lu, Chenggang Zhao, Chengqi Deng, Chenyu Zhang, Chong Ruan, et al. 2024. Deepseek-v3 technical report. *arXiv preprint arXiv:2412.19437* (2024).

Yawen Luo, Xiaoyu Shi, Jianhong Bai, Menghan Xia, Tianfan Xue, Xintao Wang, Pengfei Wan, Di Zhang, and Kun Gai. 2025. CamcloneMaster: Enabling reference-based camera control for video generation. In *Proceedings of the SIGGRAPH Asia 2025 Conference Papers*. 1–10.

Takeru Miyato, Bernhard Jaeger, Max Welling, and Andreas Geiger. 2024. GTA: A Geometry-Aware Attention Mechanism for Multi-View Transformers. In *Proceedings of the International Conference on Learning Representations (ICLR)*. OpenReview.net, Vienna, Austria, 1–18.

Norman Müller, Katja Schwarz, Barbara Rössle, Lorenzo Porzi, Samuel Rota Bulò, Matthias Nießner, and Peter Kontschieder. 2024. MultiDiff: Consistent Novel View Synthesis from a Single Image. In *Proceedings of the IEEE/CVF Conference on Computer Vision and Pattern Recognition (CVPR)*. 10258–10268.

William Peebles and Saining Xie. 2022. Scalable Diffusion Models with Transformers. *arXiv preprint arXiv:2212.09748* (2022).

QwenTeam. 2024. Qwen2.5: A Party of Foundation Models. <https://qwenlm.github.io/blog/qwen2.5/>

Xuanchi Ren, Tianchang Shen, Jiahui Huang, Huan Ling, Yifan Lu, Merlin Nimier-David, Thomas Müller, Alexander Keller, Sanja Fidler, and Jun Gao. 2025. GEN3C: 3D-Informed World-Consistent Video Generation with Precise Camera Control. *arXiv:2503.03751* [cs.CV] To appear in CVPR 2025.

Manuel-Andreas Schneider, Lukas Höller, and Matthias Nießner. 2025. WorldExplorer: Towards Generating Fully Navigable 3D Scenes. In *SIGGRAPH Asia 2025 Conference Papers*. 1–11.

Junyoung Seo, Kazumi Fukuda, Takashi Shibuya, Takuya Narihira, Naoki Murata, Shoukang Hu, Chieh-Hsin Lai, Seungryong Kim, and Yuki Mitsuji. 2024. GenWarp: Single Image to Novel Views with Semantic-Preserving Generative Warping. *arXiv preprint arXiv:2405.17251* (2024).

Xuelun Shen, Zhipeng Cai, Wei Yin, Matthias Müller, Zijun Li, Kaixuan Wang, Xiaozhi Chen, and Cheng Wang. 2024. Gim: Learning generalizable image matcher from internet videos. *arXiv preprint arXiv:2402.11095* (2024).

Oriane Siméoni, Huy V. Vo, Maximilian Seitzer, Federico Baldassarre, Maxime Oquab, Cijo Jose, Vasil Khalidov, Marc Szafraniec, Seungeun Yi, Michaël Ramamonjisoa, Franciso Massa, Daniel Haziza, Luca Wehrstedt, Jianyuan Wang, Timothée Darzet, Théo Moutakanni, Leonel Sentana, Claire Roberts, Andrea Verdaldi, Jamie Tolan, John Brandt, Camille Couprie, Julien Mairal, Hervé Jégou, Patrick Labatut, and Piotr Bojanowski. 2025. DINOV3. *arXiv preprint arXiv:2508.10104* (2025).

Jianlin Su, Yu Lu, Shengfeng Pan, Ahmed Murtadha, Bo Wen, and Yunfeng Liu. 2021. RoFormer: Enhanced Transformer with Rotary Position Embedding. *arXiv:2104.09864* [cs.CL]

Wenqiang Sun, Shuo Chen, Fangfu Liu, Zilong Chen, Yueqi Duan, Jun Zhang, and Yikai Wang. 2025. DimensionX: Create Any 3D and 4D Scenes from a Single Image with Controllable Video Diffusion. In *International Conference on Computer Vision (ICCV)*.

Hugo Touvron, Thibaut Lavril, Gautier Izacard, Xavier Martinet, Marie-Anne Lachaux, Timothée Lacroix, Baptiste Rozière, Naman Goyal, Eric Hambro, Faisal Azhar, et al. 2023. Llama: Open and efficient foundation language models. *arXiv preprint arXiv:2302.13971* (*Meta AI Technical Report*) (2023).

Thomas Unterthiner, Sjoerd Van Steenkiste, Karol Kurach, Raphael Marinier, Marcin Michalski, and Sylvain Gelly. 2018. Towards accurate generative models of video: A

new metric & challenges. *arXiv preprint arXiv:1812.01717* (2018).

Basile Van Hoorick, Rundi Wu, Ege Ozguroglu, Kyle Sargent, Ruoshi Liu, Pavel Tokmakov, Achal Dave, Changxi Zheng, and Carl Vondrick. 2024. Generative Camera Dolly: Extreme Monocular Dynamic Novel View Synthesis. *European Conference on Computer Vision (ECCV)* (2024).

Team Wan, Ang Wang, Baole Ai, Bin Wen, Chaojie Mao, Chen-Wei Xie, Di Chen, Feiwei Yu, Haiming Zhao, Jianxiao Yang, et al. 2025. Wan: Open and Advanced Large-Scale Video Generative Models. *arXiv:2503.20314 [cs.CV]*

Jianyu Wang, Minghai Chen, Nikita Karaev, Andrea Vedaldi, Christian Rupprecht, and David Novotny. 2025a. VGGT: Visual Geometry Grounded Transformer. In *Proceedings of the IEEE/CVF Conference on Computer Vision and Pattern Recognition*.

Yiming Wang, Qihang Zhang, Shengqu Cai, Tong Wu, Jan Ackermann, Zhengfei Kuang, Yang Zheng, Frano Rajic, Siyu Tang, and Gordon Wetzstein. 2025b. BulletTime: Decoupled Control of Time and Camera Pose for Video Generation. *arXiv preprint arXiv:2512.05076* (2025).

Zhouxia Wang, Ziyang Yuan, Xintao Wang, Yaowei Li, Tianshui Chen, Menghan Xia, Ping Luo, and Ying Shan. 2024. Motionctrl: A unified and flexible motion controller for video generation. In *ACM SIGGRAPH 2024 Conference Papers*. 1–11.

Tong Wu, Shuai Yang, Ryan Po, Yinghao Xu, Ziwei Liu, Dahu Lin, and Gordon Wetzstein. 2025. Video World Models with Long-term Spatial Memory. *arXiv preprint arXiv:2506.05284* (2025).

Yuhang Yang, Shukai Yin, Ke Chen, and Sifei Liu. 2025. Diffusion as Shader: 3D-aware Video Diffusion for Versatile Video Control. *arXiv:2501.03847 [cs.CV]*

Hong-Xing Yu, Haoyi Duan, Charles Herrmann, William T. Freeman, and Jiajun Wu. 2025a. WonderWorld: Interactive 3D Scene Generation from a Single Image. In *CVPR*.

Hong-Xing Yu, Haoyi Duan, Junhwa Hur, Kyle Sargent, Michael Rubinstein, William T. Freeman, Forrester Cole, Deqing Sun, Noah Snavely, Jiajun Wu, and Charles Herrmann. 2024a. Wonderjourney: Going from Anywhere to Everywhere. In *CVPR*.

Mark Yu, Wenbo Hu, Jinbo Xing, and Ying Shan. 2025b. TrajectoryCrafter: Redirecting Camera Trajectory for Monocular Videos via Diffusion Models. In *Proceedings of the IEEE/CVF International Conference on Computer Vision (ICCV)*. 100–111.

Wangbo Yu, Jinbo Xing, Li Yuan, Wenbo Hu, Xiaoyu Li, Zhipeng Huang, Xiangjun Gao, Tien-Tsin Wong, Ying Shan, and Yonghong Tian. 2024b. ViewCrafter: Taming Video Diffusion Models for High-fidelity Novel View Synthesis. *arXiv preprint arXiv:2409.02048* (2024).

Cheng Zhang, Boying Li, Meng Wei, Yan-Pei Cao, Camilo Cruz Gambardella, Dinh Phung, and Jianfei Cai. 2025b. Unified Camera Positional Encoding for Controlled Video Generation. *arXiv preprint arXiv:2512.07237* (2025).

Hongfei Zhang, Kanghao Chen, Zixin Zhang, Harold Haodong Chen, Yuanhuiyi Lyu, Yuqi Zhang, Shuai Yang, Kun Zhou, and Yingcong Chen. 2025a. DualCamCtrl: Dual-Branch Diffusion Model for Geometry-Aware Camera-Controlled Video Generation. *arXiv preprint arXiv:2511.23127* (2025).

Jensen (Jinghao) Zhou, Hang Gao, Vikram Voleti, Aaryaman Vasishta, Chun-Han Yao, Mark Boss, Philip Torr, Christian Rupprecht, and Varun Jampani. 2025. Stable Virtual Camera: Generative View Synthesis with Diffusion Models. *arXiv preprint* (2025).

## 7 Analysis of Low-Frequency Redundancy

The choice of the base frequency  $\theta = 10^4$  in video diffusion models is a legacy from RoPE embeddings used in Large Language Models (LLMs) [Su et al. 2021; Touvron et al. 2023], which often model dependencies across tens of thousands of tokens and hence require a large base frequency. However, due to using factorized RoPE, video models typically operate on a much shorter temporal context during training ( $T \approx 10$  to 128 tokens). In the temporal RoPE operator, the rotation angle increment per token for the  $f$ -th frequency band is given by  $\Delta\phi_f = \omega_f = \theta^{-2f/d_\tau}$ , where  $\theta = 10^4$ . For a typical temporal head dimension  $d_\tau = 32$ , the lowest frequency band ( $f = d_\tau/2 - 1 = 15$ ) yields a per-step rotation of  $\Delta\phi_{15} \approx 10^{-4}$  rad. Even across a maximum temporal distance of  $\Delta\tau = 100$  frames, the total phase accumulated is only  $O(10^{-2})$  rad, an amount so small that the rotation matrix is effectively the identity. This observation motivates ReRoPE to repurpose this underutilized subspace as a carrier for camera signals.

## 8 Data Annotation and Captioning Strategy

To ensure high-fidelity alignment between textual descriptions and visual content, we utilized the `caption_extend` script from the Wan2.2 pipeline for data preprocessing. Dense video captions were generated via the Qwen3-VL Plus API.

To ensure that the camera control signal is driven exclusively by our ReRoPE embeddings rather than textual correlations, we implemented a prompt construction protocol designed to decouple visual content from camera motion:

*Decoupling Camera Motion:* We explicitly filtered out descriptors related to cinematic camera movements (e.g., “pan left”, “zoom in”) from the VLM’s system prompt. This guarantees that the generated captions describe *only* the scene content and object dynamics. Consequently, the diffusion model is forced to leverage the geometric signals provided by ReRoPE, preventing “shortcut learning” through textual cues.

*Multi-View Consistency:* For the MultiCam dataset, we enforced semantic consistency across viewpoints. Given that all videos within a single scene depict the same event, we generated a caption solely for the primary view and propagated this caption to all synchronized auxiliary views. This encourages the model to interpret varying visual inputs as geometric transformations of the same semantic content, rather than as content variations.

*Handling Static Scenes:* When processing static datasets, we modified the system prompt to exclude directives regarding dynamic motion analysis. This prevents the VLM from hallucinating motion in rigid scenes (e.g., describing a static building as “moving”), thereby ensuring the text prompt accurately reflects the static nature of the environment.

## 9 Pose Estimation and Scale Unification Protocol

In the Video-to-Video (V2V) inference pipeline, we employ VIPE [Huang et al. 2025c] to extract the camera pose sequence from the source video. A primary challenge in this setting is the scale discrepancy between the estimated source trajectory (which possesses an arbitrary monocular scale) and the user-defined target trajectory.

Method	FID $\downarrow$	FVD $\downarrow$	Aesthetic Quality $\uparrow$	Imaging Quality $\uparrow$
Full-Temporal Replacement	135.4398	70.0219	0.5163	0.5757
Double RoPE	118.7149	64.2370	0.5381	0.6070
ReRoPE (Ours)	85.8568	59.4710	0.5671	0.6357

Table 4. Ablation on camera injection strategies.

To address this and ensure geometric consistency, we implement a robust two-stage normalization strategy:

1) *Individual Pre-normalization:* We first inspect the source and target trajectories independently to mitigate numerical instability caused by extreme scales. For a given trajectory  $\mathcal{T} = \{t_i\}$ , if the maximum translation magnitude exceeds a unit threshold ( $\max_i \|t_i\|_2 > 1$ ), we normalize the entire sequence by its maximum norm.

2) *Joint Normalization:* To unify the coordinate systems, we perform joint normalization on both trajectories. We define a global scaling factor  $S$  based on the union of the pre-normalized source ( $\mathcal{T}_{src}$ ) and target ( $\mathcal{T}_{tgt}$ ) trajectories:

$$S = \max_{t \in \mathcal{T}_{src} \cup \mathcal{T}_{tgt}} \|t\|_2 + \epsilon \quad (10)$$

Both trajectories are subsequently scaled by  $S$ . This ensures that the relative motion between the source and target views is preserved within a unified, model-friendly range ( $[0, 1]$ ), effectively bridging the domain gap between distinct coordinate systems.

## 10 Progressive Training Strategy

To accelerate convergence, we employ a two-stage training strategy for the V2V model. We first train on short video clips ( $T = 10$ ) to efficiently learn the camera control injection. We then load this checkpoint and resume training on longer sequences ( $T = 42$ ). This progressive scaling significantly reduces the total training duration compared to training on long contexts from scratch.

## 11 Limitations

While ReRoPE demonstrates robust 6-DoF control in static environments, its performance in Image-to-Video (I2V) settings is occasionally constrained by the inherent compositional bias of the web-scale datasets used for pre-training. Specifically, since most real-world videography tends to track salient subjects (e.g., humans) to maintain a central composition, the pre-trained backbone has acquired a strong inductive bias that couples camera movement with subject centering. This leads to an “anchoring” effect during inference: when a user-defined trajectory attempts to shift a subject away from the center or out of the frame entirely, the model’s generative prior—which favors subject visibility—often counteracts the explicit camera control signal by synthesizing compensatory subject motion. We verify that this behavior stems from data-driven semantic priors rather than architectural flaws by evaluating ReRoPE on static scenes without clear subjects, such as the DL3DV dataset. In these scenarios, our model achieves precise responsiveness to all 6-DoF target poses, confirming that the control mechanism remains highly

effective when it does not compete with strong subject-centering priors.



Fig. 8. Comparison with ablation methods.



Fig. 9. More results of camera-controlled V2V, with each row displaying a distinct camera trajectory.



Fig. 10. More results of camera-controlled I2V, with each row displaying a distinct camera trajectory.

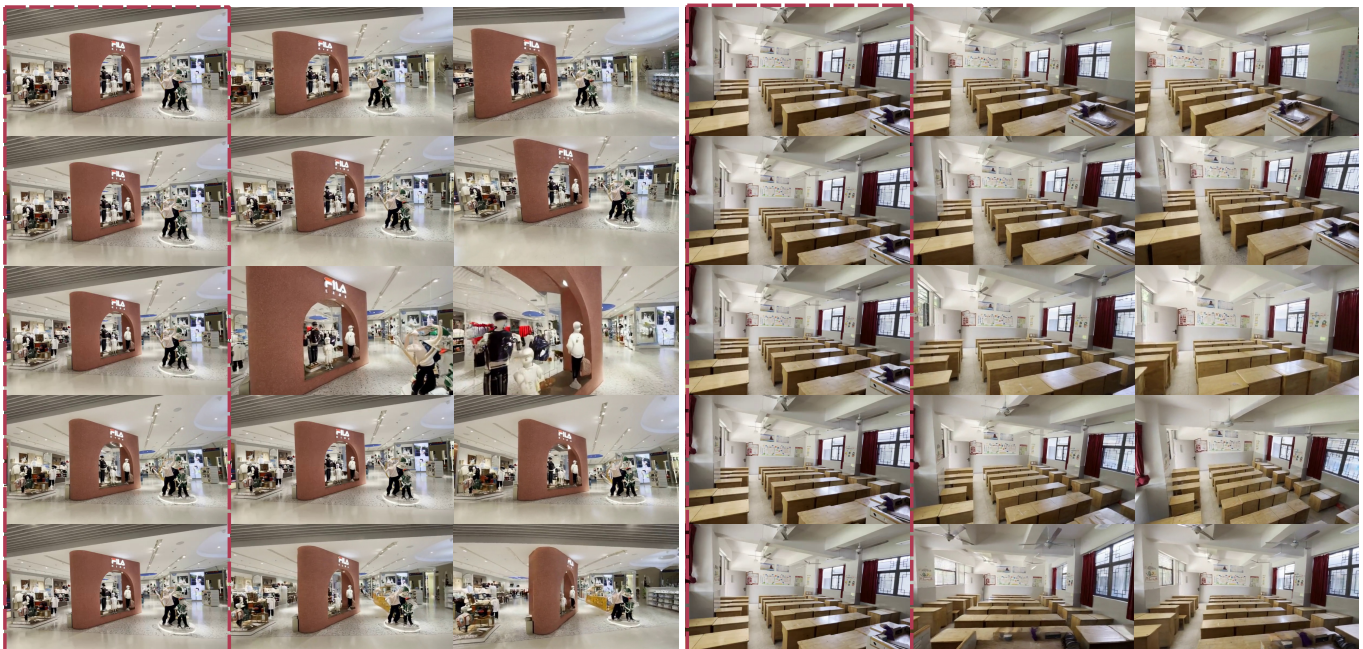


Fig. 11. More results of camera-controlled I2V on DL3DV.